NeuroImage 59 (2012) 2548–2559

Contents lists available at SciVerse ScienceDirect

NeuroImage

journal homepage: www.elsevier.com/locate/ynimg

Full-length Article

Reliable non-invasive measurement of human neurochemistry using proton spectroscopy with an anatomically defined amygdala-specific voxel

Brendon M. Nacewicz [a,1], Lisa Angelos [a,1], Kim M. Dalton [a], Ron Fischer [a], Michael J. Anderle [a], Andrew L. Alexander [a,b,c], Richard J. Davidson [a,b,d,*]

[a] Waisman Laboratory for Brain Imaging and Behavior, USA
[b] Department of Psychiatry, USA
[c] Department of Medical Physics, USA
[d] Department of Psychology, USA

ARTICLE INFO

Article history:
Received 4 March 2011
Revised 6 August 2011
Accepted 29 August 2011
Available online 5 September 2011

Keywords:
Magnetic resonance
Spectroscopy
Amygdala
Biomarker
Neurochemistry
n-aceytl-aspartate
Creatine
Choline
Inositol
Human
In-vivo
Short-echo

ABSTRACT

Given the central role of the amygdala in fear perception and expression and its likely abnormality in affective disorders and autism, there is great demand for a technique to measure differences in neurochemistry of the human amygdala. Unfortunately, it is also a technically complex target for magnetic resonance spectroscopy (MRS) due to a small volume, high field inhomogeneity and a shared boundary with hippocampus, which can undergo opposite changes in response to stress. We attempted to achieve reliable PRESS-localized single-voxel MRS at 3T of the isolated human amygdala by using anatomy to guide voxel size and location. We present data from 106 amygdala-MRS sessions from 58 volunteers aged 10 to 52 years, including two tests of one-week stability and a feasibility study in an adolescent sample. Our main outcomes were indices of spectral quality, repeated measurement variability (within- and between-subject standard deviations), and sensitivity to stable individual differences measured by intra-class correlation (ICC). We present metrics of amygdala-MRS reliability for n-acetyl-aspartate, creatine, choline, myo-Inositol, and glutamate + glutamine (Glx). We found that scan quality suffers an age-related difference in field homogeneity and modified our protocol to compensate. We further identified an effect of anatomical inclusion near the endorhinal sulcus, a region of high synaptic density, that contributes up to 29% of within-subject variability across 4 sessions (n = 14). Remaining variability in line width but not signal-to-noise also detracts from reliability. Statistical correction for partial inclusion of these strong neurochemical gradients decreases n-acetyl-aspartate reliability from an intraclass correlation of 0.84 to 0.56 for 7-minute acquisitions. This suggests that systematic differences in anatomical inclusion can contribute greatly to apparent neurochemical concentrations and could produce false group differences in experimental studies. Precise, anatomically-based prescriptions that avoid age-related sources of inhomogeneity and use longer scan times may permit study of individual differences in neurochemistry throughout development in this late-maturing structure.

Introduction

The amygdala is a core component of the social brain, indicating salience of social and emotional stimuli (e.g. Adolphs et al., 2005; Dalton et al., 2005). It is critical to emotional expression, not only of fear and anxiety (Davis and Whalen, 2001), where dendritic spine density parallels development of anxiety-like behavior from stress (Mitra et al., 2005), but also is essential to appetitive conditioning previously attributed to the dopamine system alone (Ambroggi et al., 2008). In humans, it continues to develop through late adolescence and into the middle twenties (Giedd et al., 1996, 1997; Nacewicz et al., 2006; Schumann et al., 2004) and its abnormal development has been quantitatively linked to the socio-emotional impairments of autism (Dalton et al., 2005; Munson et al., 2006; Nacewicz et al., 2006) and to the time course of depression and affective disorders (Frodl et al., 2003; McEwen, 2003; van Eijndhoven et al., 2009; Velakoulis et al., 2006).

Advances in the field of magnetic resonance spectroscopy (MRS) raise the possibility of longitudinal study of multiple, simultaneously measured neurochemicals without the radiation exposure of positron emission tomography. Non-invasive, localized proton MRS also permits prospective correlation with emotional and social behavior, a feat unachievable with post-mortem samples. A reliable MRS measurement of the amygdala could provide insight into the neuronal and glial differences that compose the gross volumetric and functional changes in normal and abnormal adolescent development, greatly advancing our understanding of this major target of psychiatric and behavioral therapy.

* Corresponding author at: Room T-225 Waisman Center, 1500 Highland Ave, University of Wisconsin-Madison, 53705, USA. Fax: +1 608 262 9440.
E-mail address: rjdavids@wisc.edu (R.J. Davidson).
[1] These authors contributed equally to this work.

1053-8119/$ – see front matter © 2011 Elsevier Inc. All rights reserved.
doi:10.1016/j.neuroimage.2011.08.090

Although current MRS techniques allow precise localization to specific brain regions, much MRS research spans swaths of cortex so large as to be almost neuroscientifically uninteresting. At an average of volume of 1.8–2.0 mL (Brierley et al., 2002), the amygdala is considerably smaller than the standard volume for spectroscopy acquisitions (typically 8 mL). A provocative finding by Oz et al. (2006) in a study of substantia nigra, an area of comparable technical difficulty, was that decreasing partial volume of adjacent tissue improved detection of a known neurochemical signature of the region. This is even more important in the medial temporal lobe, since the amygdala and hippocampus undergo opposite cytoarchitectural changes, expansion and constriction of the dendritic tree, respectively, in animal models of stress/depression (reviewed by McEwen, 2007). Recent findings in a rhesus monkey model indicate vastly different patterns of heritability for functional activation in the amygdala and hippocampus under stressful challenge conditions (Oler et al., 2010). In human work, gross volumetry reveals differential adolescent growth trajectories for amygdala and hippocampus that are also sexually dimorphic (Giedd et al., 1996, 1997). From a neuroscience perspective, it is therefore imperative to measure amygdala neurochemistry exclusive of hippocampal neurochemistry.

Neuroscientists also diverge from clinical spectroscopists in their definition of "reliability". As elegantly explained by Kreis (2004), traditional clinical studies require that the effect size of a group difference (usually a disease) be greater than the sum of within-individual variances (variance in repeatability plus between-session variance) plus between-individual variance. This approach asks the question: Are reliably resolvable peaks sufficiently stable across time, anatomy *and individuals* to see a clinically important effect? In affective neuroscience, however, sensitive detection of reliable physiological differences between healthy individuals has been used successfully to characterize behavioral traits (Tomarken et al., 1992), and these sensitive measures then used to look at pathology. This does not require the near-perfect sensitivity and specificity of single-subject diagnostics, but it requires statistical preservation of relative differences within a group (correlations). Rather than viewing it as error, this approach puts the between-individual variance in the numerator and asks the question: Are reliably resolvable peaks sufficiently stable within each individual to detect inter-individual differences that may relate to behavioral traits or adolescent development? We characterize measurement reliability first by evaluating the standard deviation of repeated measurements. This indicates overall technique capability. We then turn our attention to the ICC to relate measurement error to the size of stable between-subject differences in healthy populations.

We designed a series of studies to optimize MRS precision and sensitivity by matching the prescription to the amygdala anatomy of each participant, letting acquisition volume vary slightly but using strictly-defined criteria for spectral quality (signal to noise ratio, SNR, and spectral resolution in terms of line width of unsuppressed water, LW). We attempted to isolate amygdala from hippocampus by adapting a method from prostate chemical shift imaging, which uses a slightly overprescribed excitation volume overlapped with outer volume suppression pulses to null signal and artifact from undesired tissues (e.g. Mueller-Lisse and Scherr, 2007). We reasoned that a smaller voxel would increase anatomical precision (reduced partial volume effects) and improve shimming (see Kreis, 2004 for review), while the lower signal could be improved with additional signal averages. We validated the resultant amygdala-MRS protocol in two studies of 1-week test–retest stability. We also conducted a feasibility study to determine age-dependence of spectral quality, since our goal is a measure capable of tracking individual differences in amygdala neurochemistry during adolescent development.

Methods

Participants

Participant demographics for studies 1, 2 and 3 are listed (Table 1). All participants provided written consent or assent as part of a procedure approved by the Human Subjects Institutional Review Board of the Wisconsin School of Medicine and Public Health. Participants for study 2 were all typically developing males recruited as part of an effort to characterize amygdala neurochemistry in typical and autistic adolescent development and included 2 individuals per year of life from age 10 to 24 (two 10-year olds, two 11-year olds, etc.). Follow-up analyses were carried out on data from an additional 3 participants, aged 19.5, 19.9 and 27.2 y at the time of optimized scan, from another ongoing longitudinal study of typical and autistic adolescent amygdala development. One individual was common to studies 1 and 3, otherwise participants were unique to each study; effects in all study 3 analyses were similar with and without this individual.

Amygdala-specific MRS

Data were collected on a GE Signa 3.0 T scanner with 8-channel head coil for studies 1 and 2, and data for study 3 were collected on a GE X750 3.0 T scanner with 8-channel head coil. A system of oblique anatomical acquisitions was used to provide sagittal and axial localizers that were consistently oriented along the superior–inferior axis of the amygdala. First, a T1-weighted partial coverage scan (256× 192 matrix, resampled to 256×256, over 240 mm field of view with 64 1-mm slices; 3 m 55 s) covering the right half of the brain was acquired in an oblique sagittal plane parallel to the interhemispheric sulcus (to account for head tilt in the coronal plane and rotation in

Table 1
Sample demographics for three studies of amygdala-MRS.

	Study 1 Preliminary reliability study	Study 2 Feasibility study with children	Study 3 Optimized reliability study
Sample Size	n = 11	n = 30	n = 14
Age Mean + SD	29.3 + 9.5 y	17.3 + 4.8 y	28.9 + 6.5 y
(range)	(20.6–51.6 y)	(10.0–24.0 y)	(18.5–43.4 y)
Acquisition Volume[a]	1.85 + 0.5 cc	2.6 + 0.7 cc	2.6 + 0.3 cc
(Excitation Volume)	(2.9 + 0.9 cc)	(3.6 + 0.9 cc)	(3.2 + 0.2 cc)
GM	83 + 6%	70 + 9%	76 + 5%
WM	14 + 7%	27 + 9%	16 + 5%
CSF	3 + 2%	3 + 3%	8 + 3%
Spectral Quality	80.2 + 24	139 + 67	202 + 47
LCModel (SNR[b]/LW)			
LW	0.064 + 0.015	0.051 + 0.010	0.050 + 0.009
SNR	4.9 + 1.1	8.0 + 2.3	9.7 + 1.2

[a] Effective Acquisition Volume is Excitation Volume minus overlapping outer volume suppression bands.
[b] Signal to noise ratio for NAA methyl group calculated as (Max/[2∗$RMS_{Residual}$]) (Provencher, 1993). All values reported as mean + standard deviation. Ages are expressed in years and fractions of years.

the axial plane). A whole-brain inversion recovery-prepped T1-weighted volume (256×192 matrix, resampled to 256×256, over 240 mm field of view with 128 1-mm slices; 7 m 45 s) was prescribed off of the sagittal oblique (to preserve tilt and rotation) and angled so that the midpoint and splenium of the corpus callosum occupied the same plane. The MRS excitation volume and saturation bands were prescribed in three dimensions with simultaneous reference to both sagittal and axial localizers.

MRS excitation volumes were prescribed slightly larger than amygdalae, and then outer volume saturation bands were used in an effort to null signal from non-amygdalar tissues (Figs. 1 b, e and h). One band was placed obliquely along the posterior–inferior border of the amygdala along the alveus to null signal from the hippocampus (band 1). Another saturation band was placed anteriorly and superiorly along the dorsal margin of the amygdala and parallel to the left–right axis of the upper amygdala (band 2). A third saturation band was placed medially along the tip of the uncus in order to reduce outer volume artifacts due to sinuses (band 3). A final saturation band was placed along the anterior–inferior–lateral border (band 4).

The improved technique for study 3 involved re-orienting the posterior–inferior saturation band (band 1) by rotating the medial side anteriorly (blue arrows in Fig. 1h) and the inferior part anteriorly (blue arrows in Fig. 1e) until it covered the corner of the excitation volume closest to the auditory canal. The medial saturation band (band 3) was also adjusted to cover the corner closest to the auditory canal by moving the inferior portion laterally (blue arrows in Fig. 1b) and the posterior portion laterally (blue arrows in Fig. 1h). The improvement in spectral quality (See Results and Table 1) from this modification attests to the efficacy of using outer volume saturation bands to null unwanted signal in an overprescribed excitation volume.

Spectroscopic data were acquired using point-resolved spectroscopy (PRESS) with echo time (TE) 35 ms and repetition time (TR) 1.5 s and 256 averages of 4096 complex data points plus 16 acquisitions without water suppression (time: 7 m 0 s). While longer TRs

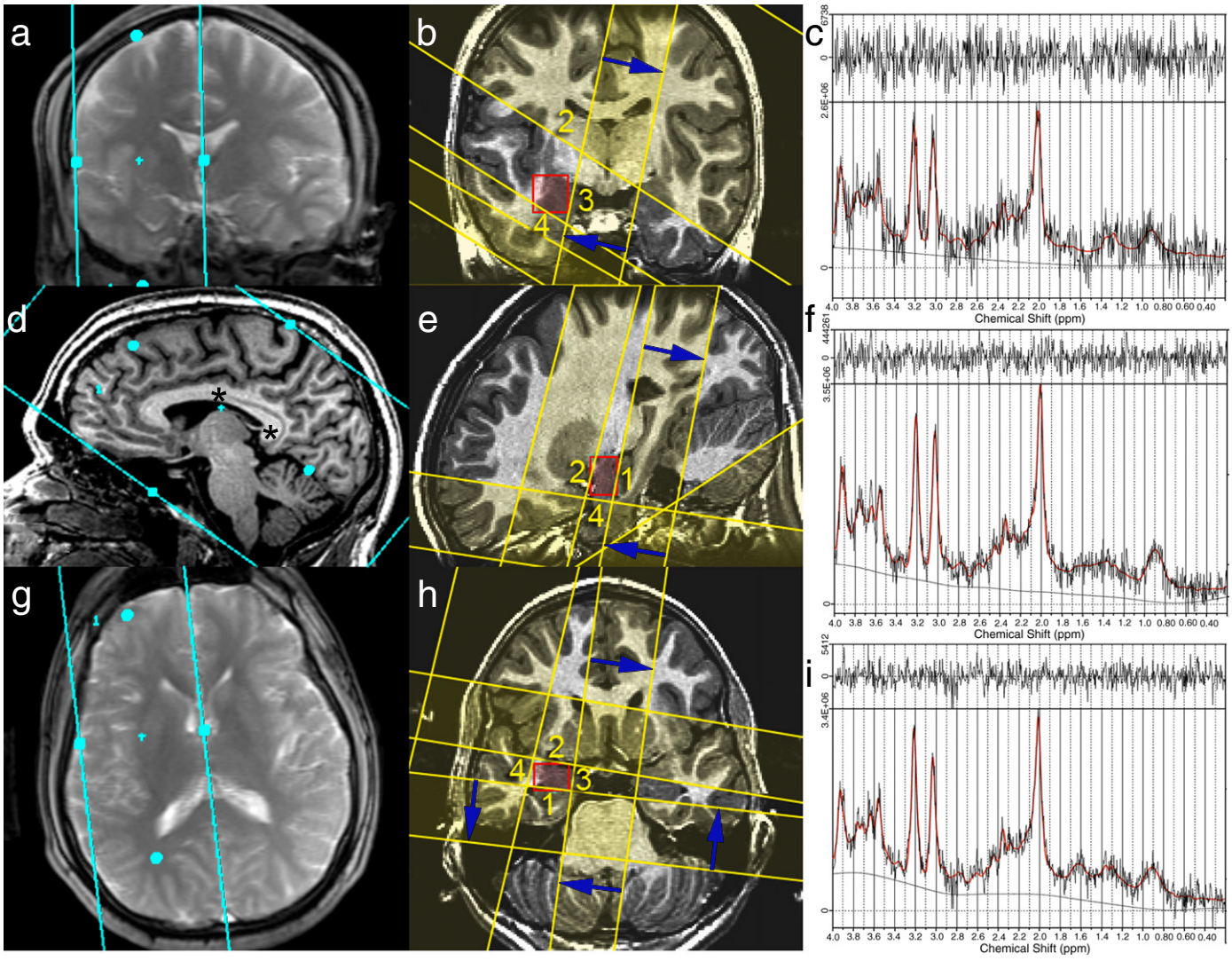

Fig. 1. Amygdala-specific MRS protocol and example spectra. Anatomical localizers include a partial coverage sagittal acquisition oriented along the cerebral falx in coronal (a) and axial (g) views to correct for head tilt and rotation, respectively (Teal lines indicate bounds of acquisition). A full coverage anatomical image is then prescribed off the oblique sagittal localizer (d) and oriented obliquely to parallel the angle formed by the midpoint and splenium of the corpus callosum (asterisks), which tends to be normal to the S–I axis of the amygdala. For the MRS prescription, the excitation volume (red box) is overlaid on coronal (b), sagittal (e) and axial (h) anatomical images, showing isolation of right amygdala (left = right). Further separation from surrounding tissues is achieved with four oblique outer volume suppression bands (numbered yellow regions) as follows: band 1 is placed along the alveus to ensure separation from hippocampus; band 2 is placed on the superior surface to reduce flow artifact from middle cerebral artery and signal from caudate/putamen; band 3 reduces susceptibility artifact due to perinasal sinuses and temporal airspaces; band 4 follows the inferior anterolateral border of amygdala. Blue arrows indicate adjustments for optimized homogeneity used in study 3. Individual spectrum representative of mean spectral quality for study 1 (c, LW = 0.062 ppm, SNR = 5), representative spectrum of mean spectral quality for *children* in study 2 (f, LW = 0.053 ppm, SNR = 10), and representative spectrum of mean spectral quality for study 3 (i, LW = 0.048 ppm, SNR = 10).

potentially permit more T1 relaxation and are essential for efforts at absolute quantitation, we found little improvement in spectral quality with TRs>1.5 s. We optimized field homogeneity by automated linear shimming and manual repositioning of the excitation volume. Automated high order shimming over the whole brain or right hemisphere specifically provided no improvement over linear shims alone. For all studies, iterative voxel adjustment was carried out to afford the largest excitation volume possible (at least 3 mL for study 3) that could be shimmed to a pre-scan line width (LW; full-width at half maximum) of 9 Hz or less (0.070 ppm) as recommended (Kreis, 2004). In study 1, since the major source of field inhomogeneity had not yet been identified and avoided, excitation volumes tended to be smaller to facilitate shimming to the required LW. Smaller volumes led to poorer signal to noise ratios (SNR), so subsequent studies were required to meet both the pre-scan LW criterion and the further requirement that post-scan LCModel output showed SNR/LW>=100. This provides an excellent cost function since SNR increases but LW also increases for larger volumes in regions of high magnetic field inhomogeneity. All spectra were analyzed with LCModel with water scaling and eddy current correction based on the unsuppressed acquisitions.

Acquisition volume reconstruction

Masks corresponding to the spectroscopy excitation volume and the four outer volume saturation bands were created in anatomical space using in-house software written in Perl and Python. Geometric information about the anatomical images (anatomical volume size, resolution, position, and orientation) was read from the image header using in-house software written in Python. Geometric information about the spectroscopy excitation voxel (size, location, and orientation) and outer volume saturation bands (offset, thickness, and normal vector) were read from the spectroscopy data file using GE's SAGE package (spectroscopy analysis by GE). The spectroscopy excitation volume and the four saturation bands were reconstructed in anatomical space as binary masks, and the effective acquisition volume was calculated as excitation volume $(1-\text{sat1})\times(1-\text{sat2})\times(1-\text{sat3})\times(1-\text{sat4})$.

Anatomical preprocessing and segmentation

Segmentation of brain tissue compartments (GM, WM, CSF) was carried out on the axial T1-weighted anatomical images using a custom procedure designed to optimize segmentation in the area of the amygdala. This procedure used 3dSkullStrip (Cox, 1996) to remove skull, then brains were corrected for intensity bias using tissue segmentation with spatial priors in FSL's FAST routine (http://www.fmrib.ox.ac.uk/fsl). The resultant image was automatically scaled (contrast adjusted) so that the peak of the white matter histogram (mode of white matter intensity) was at 80% of the 16-bit range using in-house software (written in Python) and AFNI's 3dcalc tool. Image intensities were then squared for optimal peak separation and contrast adjustment was repeated. The resultant images were then segmented using FAST with spatial priors. This procedure produces images with superb separation of all tissue types and optimizes contrast for viewing variations in the gray matter distribution.

Neurochemical estimates were corrected based on the assumption of negligible contributions from CSF due to low concentrations and high T2 values. All neurochemical concentrations were corrected as $[\text{chemical}]/(1-\text{CSF}_{\text{fraction}})$ as described previously to yield measurements in arbitrary units (e.g. Port et al., 2008). Investigators seeking absolute concentrations of neurochemicals often correct for differential relaxation in gray and white matter, assuming neurochemical relaxation times are similar throughout gray matter and white matter and assuming approximately uniform neurochemical concentrations. Since our experimental objectives do not require absolute concentrations, this correction was not carried out, but mean tissue components of acquisition volumes are included for each study (Table 1) so that readers may perform these calculations as they see fit or as consensus emerges for the prerequisite neurochemical properties.

Within-subject unbiased coregistration and reliability

For study 1, between-session reproducibility of the acquisition volume placement was calculated as a spatial overlap measure. Anatomical images from time 1 and time 2 scans were processed as for tissue segmentation (above) and then coregistered. Since a simple transformation and resampling of one time point to the other would cause partial voluming and effective dilation in one MRS mask but not the other, we devised a procedure to equally distribute partial volume effects. Using a linear transformation with six degrees of freedom (rigid body transform) in FLIRT, the time 1–>2 transformation was calculated, then the time 2–>1 transformation was calculated and reversed, these transformations were averaged to create an unbiased time 1–>2 transformation and then halved. This half transformation was applied to the time 1 image and the reverse transformation was applied to the time 2 image and the resultant images were averaged to create a composite exactly half way along the transformation between the two time points. Effective MRS acquisition volumes were transformed using the unbiased transformations from the anatomical images and all non-zero voxels were used to calculate the spatial reliability as intersection/union. Although this likely is an underestimate of the true reliability because of the inherent dilation due to partial volume effects, the average spatial reliability of 0.58 ± 0.06 ($n=11$) was excellent for this type of procedure (compare with intersection/union of 0.80–0.85 for various hand-drawn amygdala region of interest studies; e.g. Nacewicz et al., 2006; Rojas et al., 2004).

For study 3, since each individual had 4 sessions, a relatively equidistant average was calculated using the above procedure serially on sessions 1 and 2, sessions 3 and 4, and then on the two midpoints. The resultant anatomy can be seen in Figs. 5(c–e). As in study 1, effective acquisition volume masks were transformed to the same space for comparison relative to each individual's own brain anatomy. Extent in each direction was extracted from i, j, and k matrices of the RAI-oriented images using AFNI's 3dCalc. For the within-subject analyses, only between-session differences in spatial extent were used, which obviated the need for coregistration between subjects. For the between-subject analyses, the L–R and S–I coordinates of the most medial extent of the semiannular sulcus were identified on each individual's 4-session average image as an indentation proximal to the optic tract. The medial coordinate (i) was defined as the first sagittal plane after the largest decrease in tissue area moving laterally to medially through the area of the semilunar gyrus beneath the optic tract. The inferior coordinate (k) was defined as the first axial plane after the largest decrease in tissue area moving inferiorly to superiorly. Similarly, L–R and S–I coordinates were estimated for the semilunar gyrus at the point of furthest superomedial extent in coronal view and the furthest anteromedial extent in axial view.

Field map reconstruction and coregistration

Field maps for study 2 were generated from axial 2D gradient echo scans (128×128 matrix over a 240 mm field of view and 46 3-mm slices) acquired with echo times of 7 ms and 10 ms. Reconstruction, phase-unwrapping and field map calculation was performed with Prelude (FSL). These were then coregistered to the oblique anatomicals using FLIRT (FSL) with a restricted "coarsesearch" (-10 to $10°$) in order to accommodate variability from partial coverage of superior and inferior edges. Images were then multiplied by binary masks of the effective MRS volume for analysis of within-volume field inhomogeneity (intensity variance).

Statistical analyses

Statistical analyses were carried out with the Statistica (Statsoft, Tulsa, OK) software package. Intraclass correlations were calculated as Shrout and Fliess model 1 (Shrout and Fleiss, 1979). We controlled for multiple comparisons by entering all variables of interest for each study into a single general linear model; zero-order correlations are depicted for the sake of illustration.

Results

Amygdala-specific spectroscopy procedure and reliability

All published MRS studies of the amygdala use an acquisition volume of fixed dimensions that includes a variable amount of hippocampus and other potential sources of artifact. We took an alternate approach: we varied the acquisition volume to match the shape of the amygdala for each individual, based on expertise from amygdala morphometry, and kept strict standards for spectral quality. We immediately ruled out chemical shift imaging (CSI), due to poor local shimming in the region. We did, however, adapt a prostate CSI technique for use with a single voxel, slightly over-prescribing the excitation volume to encompass the amygdala and some surrounding tissue, and then using outer volume suppression bands to null signal from unwanted tissues and sources of artifact (Figs. 1b, e, and h). The amygdala MRS prescription was adjusted until pre-scan showed a line width of 9 Hz (0.070 ppm) or less. Acquisitions were immediately processed in LCModel, and prescriptions were iteratively adjusted during the acquisition session if they did not meet spectral quality standards. Acquisition volumes and spectral quality data are listed (Table 1).

Our goal was the shortest possible scanner time both because we aim to use this technique on children and populations with developmental disabilities and because our anticipated gains from anatomical precision could be reversed by subject motion over a long scan. After testing several combinations of relaxation time and signal averages, we reasoned that the estimates achieved at the partially relaxed TR = 1.5 s with 256 averages gave a good tradeoff between scan-time and data quality. As expected (Drost et al., 2002), PRESS produced greater signal than STEAM and shorter echo time (TE = 35 ms) preserved greater SNR than longer echo time (TE = 144 ms) in this difficult to image region. Global high order shim added nothing to spectral quality over standard (automated) linear shimming, and was therefore abandoned. We improved voxel setup time by correcting for head rotation in all three planes through two multiply-oblique localizers that approximated the superior–inferior axis of the amygdala while giving us three-dimensional information for the prescription. With practice, the entire session, including anatomical localizer images and a 7-minute amygdala-MRS, could be completed in approximately 25 min.

Study 1: Initial reliability study

Although still noisier than other brain regions, we deemed our amygdala spectra to be of sufficient quality for a preliminary test of short-term reliability. In study 1, we assessed 13 individuals in two scanning sessions a week apart (mean inter-scan interval 7.6 days) and were able to get useable spectra (pre-scan LW < 0.070 ppm) on 11 of them (Table 2, study 1). All of the major metabolites had a goodness of fit generally accepted as reliable for interpretation at the single-subject level (CRLB < 20%). We found significant intraclass correlations for the ubiquitous energy storage molecule creatine (Cre), the neuron-specific amino–acid derivative n-acetyl-aspartate (NAA; representing NAA + NAAG since NAAG was not reliably detected), and membrane precursor cholines (Cho). The metabolites myo-Inositol (mI) and glutamine + glutamate (Glx) had good fit statistics but showed poor reliability (ICC) (Table 2, study 1).

We observed that our best qualitative fit in regions of coupled resonances and best fit statistics (CRLB < 20% for Glx) were not simply related to either LW or SNR but seemed to require a threshold post-scan of (LCModel estimated) LW < 0.07 ppm and SNR/LW greater than 100. The aim of this cost function is to prevent deterioration of SNR due to excessively small volumes that are easily shimmed. For studies 2 and 3, we used these as inclusion criteria.

Study 2: Age-related differences in spectral quality from age 10 to mid-adulthood

We then turned our attention to using the technique in children, in order to see if these criteria were at all realistic. As part of a study of adolescent amygdala development to be described elsewhere, we collected amygdala-MRS from 30 males (Table 1, study 2) with a uniform age distribution from age 10 to 24 (e.g. two 10-year-olds, two 11-year-olds, etc.). Our first attempts at scanning younger children completely defied our expectations: the initial pre-scan LW and resultant spectra were considerably better than those from adults.

Despite continued ease of scanning in children, we failed to achieve our strict pre-scan LW limit of 0.070 ppm in an undesirably high eight of 30 individuals. Looking quantitatively at data from the 22 subjects who met our inclusion criteria, we found a trend towards better spectral quality (SNR/LW) in younger children ($r = -0.40$, $p = 0.06$), driven by a significant negative relationship between age

Table 2
One week reliability of metabolite estimates from study 1 and study 3.

	Study 1					Study 3				
	Mean CRLB% (range)	Mean (A.U.)	Within-individual SD[a]	Between-individual SD[b]	Reliability ICC	Mean CRLB % (range)	Mean (A.U.)	Within-individual SD[a]	Between-individual SD[b]	Reliability ICC
NAA	7.5%	7.5	0.86	1.35	0.52	5.2%	8.5	0.71	1.38	0.69
	(5–10)		11.5%	18.0%	$p = 0.04$	(4–8)		8.4%	16.2%	$p = 7\times10^{-9}$
Cre	6.8%	6.5	0.60	1.00	0.56	4.1%	7.4	0.58	0.99	0.58
	(5–9)		9.2%	15.4%	$p = 0.02$	(3–5)		7.8%	13.4%	$p = 2\times10^{-6}$
Cho	5.4%	2.9	0.25	0.41	0.54	3.5%	3.0	0.21	0.41	0.70
	(4–9)		8.6%	14.1%	$p = 0.03$	(3–5)		7.0%	13.7%	$p = 2\times10^{-9}$
mI	10.2%	6.9	0.82	1.23	0.36	6.7%	7.1	0.78	1.25	0.55
	(7–14)		11.9%	17.8%	$p = 0.11$	(5–10)		11.0%	17.6%	$p = 5\times10^{-6}$
Glx	13.8%	15.3	2.36	3.08	0.29	9.7%	16.3	2.66	3.31	0.24
	(10–22)		15.4%	20.1%	$p = 0.17$	(6–16)		16.3%	20.3%	$p = 0.02$

[a] Within-Individual SD calculated as the average across all individuals of the within-individual SDs across the four sessions.
[b] Between-Individual SD calculated as the average across the four sessions of the within-session between-individual SDs. NAA indicates NAA + NAAG; Cho, GPC + PCh; Glx, Glu + Gln + GSH; ICC, intraclass correlation.

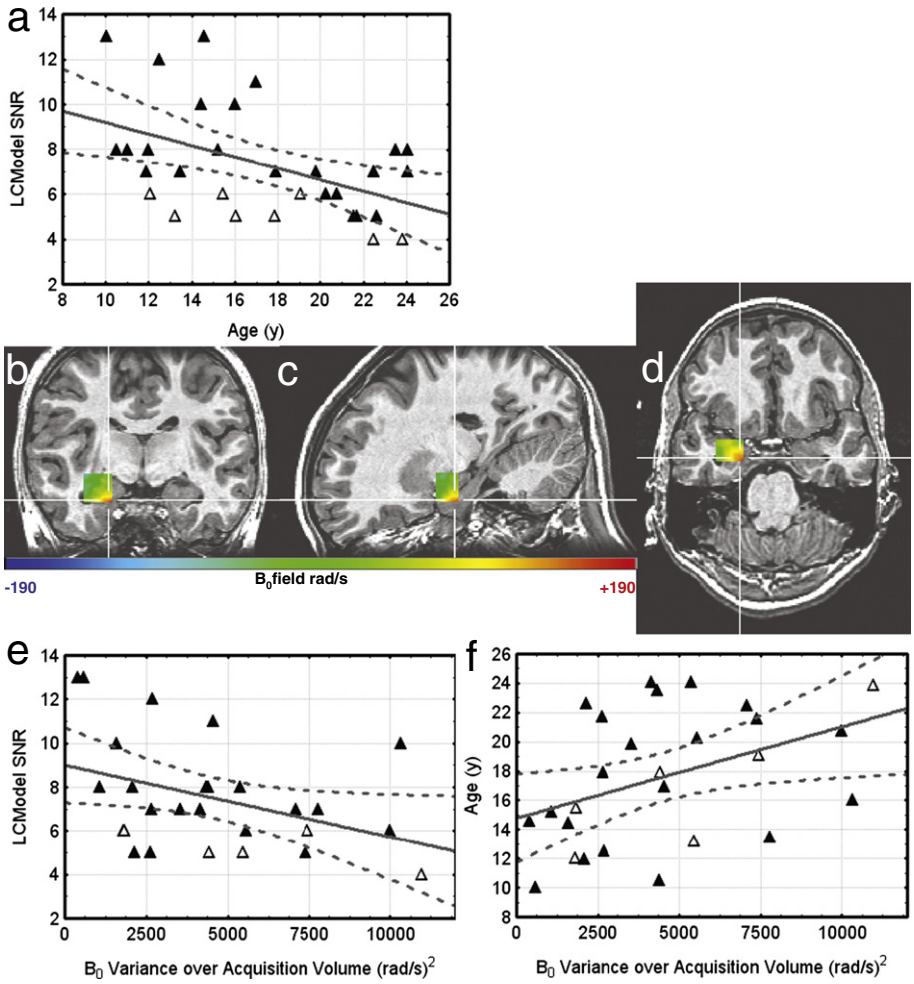

Fig. 2. Age-related difference in spectral quality is likely due to internal auditory canal and mastoid development, not perinasal sinus development. Plot of best-achieved dataset for each individual (a, e–f), including those failing to meet our rejection criteria (open triangles), shows better signal to noise in younger children (a, $r = -0.48$, $p = 0.007$). Analysis of B_0 field map masked with excitation volume (b–d) shows a sharp field deflection in posterior–inferior–medial corner, closest to the internal auditory canal. Variance in B_0 across acquisition volume is inversely correlated with SNR, $r = -0.39$, $p = 0.04$, (e) and positively correlated with age, $r = 0.41$, $p = 0.03$ (f).

and SNR ($r = -0.56$, $p = 0.006$) that persists when all 30 datasets are examined (Fig. 2a). Post-hoc examination of B_0 field maps revealed that peri-nasal sinuses contributed some inhomogeneity, but the overwhelming pattern was a steep deflection in the inferior–medial–posterior corner as in the example (Figs. 2b–d) that sharply reversed at the edge of the internal auditory canal (Supplementary Fig. 1). Variance in the B_0 field over the acquisition volume quantitatively linked SNR (Fig. 2e) and age (Fig. 2f).

The amygdala-MRS procedure was adapted to avoid this corner (Fig. 1, blue arrows). This likely contributes to the 153% improvement in spectral quality (SNR/LW) from study 1 to study 3 (Table 1), with a nearly identical improvement of 154% from 88 to 224 for one individual from study 1, aged 43.4 y, who elected to participate in study 3 as a quality control check. Study 3 was carried out on a different scanner, however, which also likely contributed to improved spectral quality. To measure the proportional improvement from our technique, we examined data from 3 individuals from an ongoing longitudinal study whose initial amygdala-MRS sessions were particularly bad and who were willing to be rescanned with the improved technique before the scanner was replaced. Mean spectral quality (SNR/LW) improved by 123% from 57 to 138 (paired $T_3 = 6.5$, $p = 0.007$), driven by an improvement in mean LW from 0.114 ppm to 0.056 ppm (paired $T_3 = 3.8$, $p = 0.03$). This suggests that avoidance of the internal auditory canal alone confers a striking improvement in spectral quality.

Study 3: Improved spectral quality and reliability with optimized amygdala-MRS

Optimized amygdala-MRS allowed LW from adults that matched that of children from study 2 with superior SNR (Fig. 1i, Table 1). To examine reliability, 14 participants underwent 4 sessions divided as morning and evening scans on 2 different days, 1 week apart. A mixed general linear model with week and time of day as random and fixed effects, respectively, showed no significant effect of time of day or of scan week for any major metabolite, so all 4 sessions were subsequently treated equivalently. Within-subject coefficients of variation for NAA, Cre, Cho, and mI were reduced with the new technique and intraclass correlations across all 4 sessions were much improved (Table 2), with pairwise intraclass correlations as high as 0.81 for NAA.

One concern with an anatomically defined voxel in a region of high field inhomogeneity is the possibility that systematic differences in spectral quality may dominate the between-subject variation of measurements, inflating ICCs. We therefore took advantage of the within-subject variation across 4 separate sessions to determine whether differences in measures of spectral quality, acquisition volume, or tissue content systematically related to variability in metabolite estimates. We looked at 4-session single-subject metabolite standard deviation, an absolute measure, and found no relationship with the

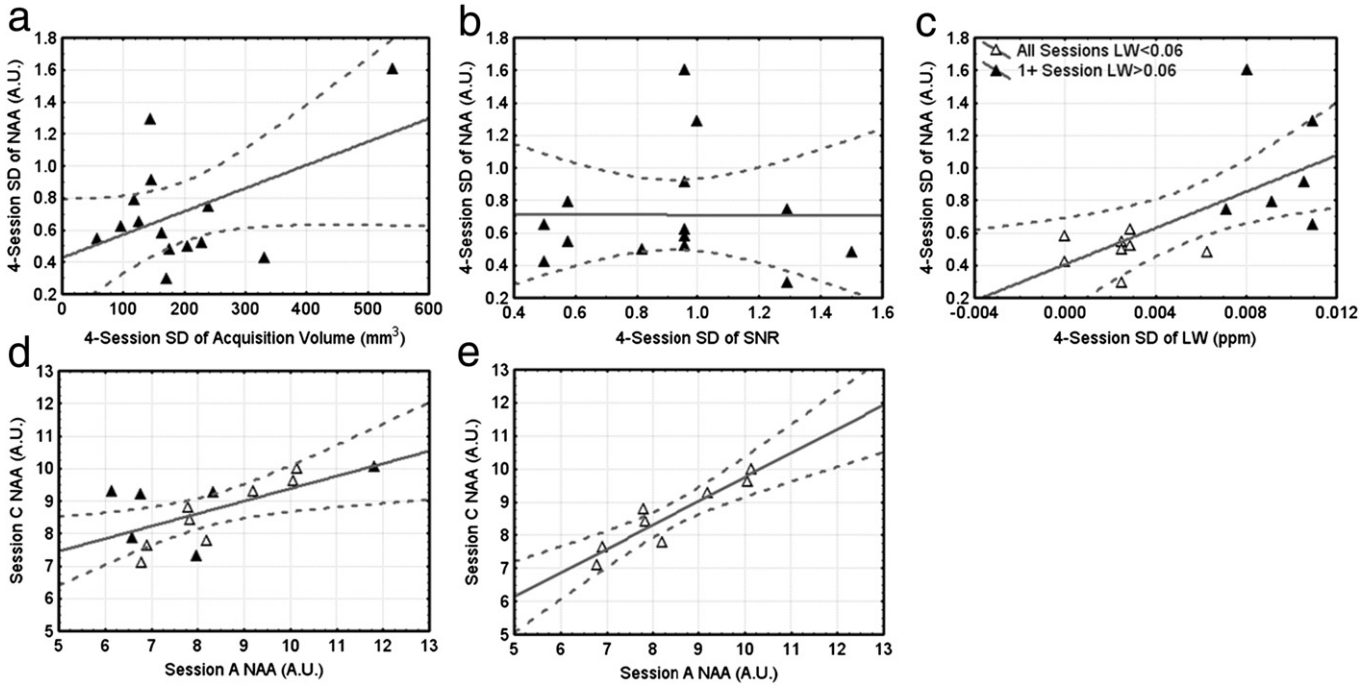

Fig. 3. Reliability is not due to systematic differences in volume or spectral quality. Comparison of standard deviation across all four sessions for NAA reveal essentially no influence of acquisition volume (a, $r = 0.50$, $p = 0.07$; without outlier $r = -0.09$, $p = 0.8$) or signal-to-noise ratio (SNR;b, $r = 0.03$, $p = 0.9$). A similar comparison with line width (LW) reveals a positive correlation (c, $r = 0.66$, $p = 0.01$). Considering only participants where all 4 sessions had LW<0.06 ($n = 8$, open triangles), line width no longer influenced variability in NAA ($r = 0.07$, $p = 0.9$). Examining the sessions with poorest 2-session reliability for CSF-corrected NAA estimates (d, ICC = 0.53, $p = 0.02$), we found that including only those subjects with LW<0.06 ppm for both sessions ($n = 8$, e) improved the 2-session reliability (ICC = 0.89, $p = 2 \times 10^{-4}$). Similar results obtain for Cre and Cho but not mI or Glx (not shown).

standard deviation of acquisition volume or SNR (Figs. 3a, b). Although LW was improved in study 3 (Table 1), the known relationship between absolute differences in LW and metabolite estimates (e.g. Geurts et al., 2004) remained significant (Fig. 3c). By excluding participants with any single session LW above 0.06 ppm, this effect was no longer apparent (Fig. 3c, open triangles). We revisited our intraclass correlations with this more stringent criterion and found improved reliability in NAA, Cho, Cre, and Glx estimates (Table 3). Examining sessions in a pair-wise fashion, the stronger correlations were largely unaffected by restricting LW, but the poorest pairings showed drastic improvements (Figs. 3d, e). It should be noted that an increased LW can lead to both over- and under-estimation of NAA, rendering a simple linear correction useless.

In addition to comparisons of standard deviation, we carried out comparisons using signed within-subject change from the first session (session A) calculated for the remaining three sessions (sessions B–D). We tested change in each metabolite in a mixed general linear model with session as a random factor and found no effect of change in acquisition volume or SNR (data not shown). A positive correlation with change in gray-matter/white-matter fraction (GM/WM) was evident only for change in Cho ($F_{1,38} = 15$); residualizing estimated Cho on GM/WM across all sessions produced a nearly identical reliability (ICC = 0.72, $p = 8 \times 10^{-10}$) to the uncorrected reliability (ICC = 0.70; Table 3). These data affirm that reliability of amygdala-MRS is not due to systematic differences in scan quality.

Effects of anatomical position on within-individual variation

Another possibility is that individual differences in sampled anatomy, due to size and shape of a given amygdala, underlie the reliability (ICC).

Table 3
Four-session (study 3) metabolite reliability, including 1-week stability using optimized amygdala-MRS.

	Basic processing (CSF correction only)				Spatial correction			Ideal[c] (n = 8)
	Within-individual SD[a]	Between-individual SD[b]	Reliability ICC	LW<0.06 ppm reliability ICC (n = 8)	Within-individual SD[a]	Between-individual SD[b]	Reliability ICC	Reliability ICC
NAA	0.71	1.38	0.69	0.84	0.58	0.89	0.55	0.56
	8.4%	16.2%	$p = 7 \times 10^{-9}$	$p = 7 \times 10^{-9}$	6.8%	10.5%	$p = 5.1 \times 10^{-6}$	$p = 0.0004$
Cre	0.58	0.99	0.58	0.74	0.42	0.66	0.58	0.52
	7.8%	13.4%	$p = 2 \times 10^{-6}$	$p = 1 \times 10^{-6}$	5.7%	8.9%	$p = 1.6 \times 10^{-6}$	$p = 0.0009$
Cho	0.21	0.41	0.70	0.74	0.26	0.36	0.70	0.07
	7.0%	13.7%	$p = 2 \times 10^{-9}$	$p = 1 \times 10^{-6}$	8.7%	11.9%	$p = 2.5 \times 10^{-9}$	$p = 0.28$
mI	0.78	1.25	0.55	0.42	0.79	1.24	0.44	0.31
	11.0%	17.6%	$p = 5 \times 10^{-6}$	$p = 0.006$	11.1%	17.5%	$p = 2.4 \times 10^{-4}$	$p = 0.03$
Glx	2.66	3.31	0.24	0.31	1.74	2.31	0.28	0.25
	16.3%	20.3%	$p = 0.02$	$p = 0.03$	10.7%	14.2%	$p = 0.010$	$p = 0.06$

[a] Within-Individual SD calculated as the average across all individuals of the within-individual SDs across the four sessions.
[b] Between-Individual SD calculated as the average across the four sessions of the within-session between-individual SDs.
[c] Residual SAS-corrected estimates with line width<0.06 ppm regressed on gray matter/white matter fraction (GM/WM) across all sessions and individuals. LW indicates line width; SD, standard deviation; ICC, intraclass correlation; SAS, semiannular sulcus.

Table 4
Within-individual variation in anatomical position of MRS acquisition across four sessions systematically influences metabolite estimates.

Metabolite	Lateral	Medial	Anterior	Posterior	Inferior	Superior
NAA	$\beta = -0.12$ $r_{semi} = -0.07$	$\beta = 0.45$ $r_{semi} = 0.28$ $p = 0.04$	$\beta = 0.05$ $r_{semi} = 0.04$	$\beta = -0.09$ $r_{semi} = -0.07$	$\beta = 0.39$ $r_{semi} = 0.29$ $p = 0.04$	$\beta = -0.28$ $r_{semi} = -0.22$ $p = 0.10$
Cre	$\beta = -0.21$ $r_{semi} = -0.14$ $p = 0.20$	$\beta = 0.87$ $r_{semi} = 0.54$ $p = 1 \times 10^{-5}$	$\beta = -0.19$ $r_{semi} = -0.13$	$\beta = 0.07$ $r_{semi} = 0.05$	$\beta = 0.28$ $r_{semi} = 0.21$ $p = 0.06$	$\beta = -0.12$ $r_{semi} = -0.10$
Cho	$\beta = 0.07$ $r_{semi} = 0.04$	$\beta = 0.66$ $r_{semi} = 0.41$ $p = 0.002$	$\beta = -0.44$ $r_{semi} = -0.29$ $p = 0.02$	$\beta = 0.17$ $r_{semi} = 0.12$	$\beta = 0.37$ $r_{semi} = 0.28$ $p = 0.03$	$\beta = -0.27$ $r_{semi} = -0.21$ $p = 0.09$
mI	$\beta = -0.02$ $r_{semi} = -0.01$	$\beta = 0.27$ $r_{semi} = 0.17$	$\beta = 0.10$ $r_{semi} = 0.07$	$\beta = 0.04$ $r_{semi} = 0.03$	$\beta = -0.31$ $r_{semi} = 0.23$ $p = 0.15$	$\beta = -0.17$ $r_{semi} = -0.14$
Glx	$\beta = -0.61$ $r_{semi} = -0.40$ $p = 0.006$	$\beta = 0.62$ $r_{semi} = 0.38$ $p = 0.009$	$\beta = -0.31$ $r_{semi} = -0.21$ $p = 0.14$	$\beta = 0.11$ $r_{semi} = 0.07$	$\beta = 0.20$ $r_{semi} = 0.15$	$\beta = -0.16$ $r_{semi} = -0.13$

$p > 0.20$ not shown; Directionality follows RAI-based coordinate system: higher Lateral and Medial values indicate more medial placement, higher Anterior and Posterior values indicate more posterior placement; higher Inferior and Superior values indicate more superior placement.

Our optimized method with nulling of artifact from the inferior auditory canal was so effective that good LW was achievable over a broader portion of the uncus, allowing greater variability of acquisition volume position in study 3. This within-subject variability across sessions allowed us to conduct a post-hoc quantitative test of the contribution of variable anatomical location to metabolite estimates. Anatomical images from all four sessions were coregistered, then minimal and maximal extents in all three cardinal directions were extracted from this anatomically aligned space for each individual and session. Signed differences from session A were calculated as above to test, at the group level, the hypothesis that systematic differences in spatial positioning relative to individual anatomy affect chemical estimates. All six extent parameters were entered into a general linear model with session as a random variable to test contributions to each metabolite estimate (Table 4). Interestingly, a pattern emerged of proportionally greater metabolite estimates when the acquisition volume extended further medially. This pattern was particularly prominent for Cre and Cho (Figs. 4a–c), accounting for 29% of the unique within-individual variance in Cre (Table 4). An additional pattern of greater metabolite estimates with less extensive inferior coverage (more superior termination) was significant for NAA and Cho and trend level ($p = 0.06$) for Cre. Examination of scatterplots (Figs. 4d–f) suggests non-linear effects with larger variations in the inferior boarder. Additionally, Cho but not NAA or Cre also shows a significant influence of anterior border with greater Cho when the acquisition extends more anteriorly (Table 4).

We wondered whether these differences in extent mapped to a known factor influencing MRS estimates. We therefore simultaneously covaried medial, inferior and anterior extent along with SNR, LW and

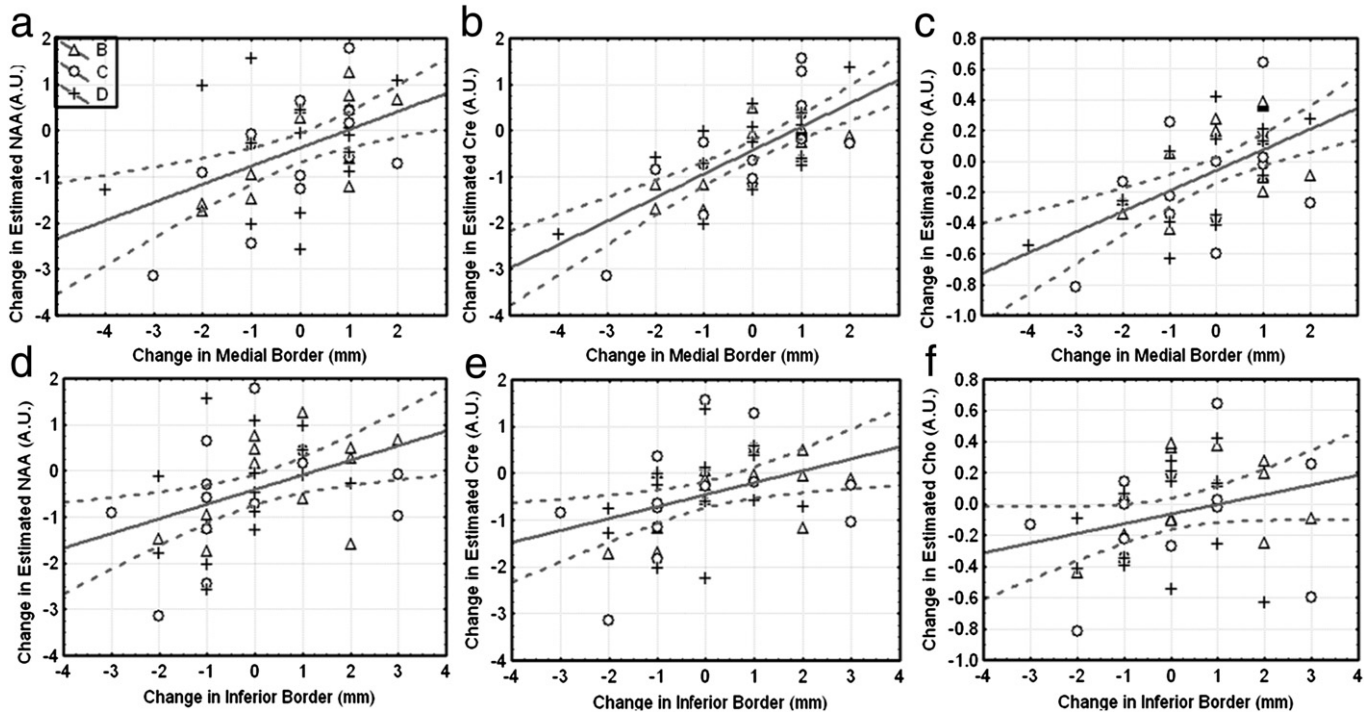

Fig. 4. Within-individual variability in metabolite estimates across four sessions correlates with anatomical location of medial (a–c) and inferior (d–f) border of MRS prescription. After coregistration of all sessions, differences between the first session and subsequent sessions were calculated for minimal and maximal extent in each cardinal direction and compared with between session changes in metabolite estimates. Higher values for the medial border indicate more medial coverage and produce increases in estimated NAA (a, zero-order $r = 0.47$, $p = 0.002$), Cre (b, $r = 0.72$, $p = 8 \times 10^{-8}$), and Cho (c, $r = 0.56$, $p = 0.001$). Higher values for the inferior border indicate more superior termination (less inferior coverage) and produce increased estimates of NAA (d, $r = 0.40$, $p = 0.008$) and Cre (e, $r = 0.38$, $p = 0.01$), with a nonsignificant relationship with Cho (f, $r = 0.28$, $p = 0.08$). Symbols depict within-individual difference between MRS session A and subsequent sessions B—D.

GM/WM in a mixed model with session as a random variable (Table 5). Medial and inferior extent continued to influence metabolite estimates, although the relationship of medial extent and NAA fell from significance. Interestingly, dependence of Cho estimates on anterior extent was eliminated by inclusion of tissue content (GM/WM), suggesting a partial volume effect.

Given the robustness of the relationships, particularly of medial and inferior border extent, with the metabolite estimates, we attempted to normalize estimates based on the metabolite-specific slopes (beta values) generated by regressing change in metabolite on change in medial and inferior border in a mixed model with session as a random variable. Session B–D estimates were then extrapolated to the spatial extent of Session A, using these group–derived slopes with each individual difference in medial and inferior extent for each session. This attempt at spatial correction reduced the within–subject metabolite variation substantially, accounting for 20–30% of the within-subject standard deviation for NAA and Cre (Table 3). These data show that variable inclusion of medial and inferior tissue has a pronounced effect on metabolite estimates. In particular, the variation in Cre with medial border was larger (21%) than the variation of Cho with tissue content (18%) (Table 5). This shows that, in the amygdala region, the details of voxel placement relative to anatomy are as important as the more commonly observed partial volume (GM/WM fraction) effect.

Medial and inferior borders vary over region of high neural density

The above analyses suggest that strong spatial gradients in neurochemistry may exist around the borders of our amygdala-MRS acquisition, but with the curious finding that more medial tissue produces higher estimates while more inferior tissue produces lower estimates. Sutoo et al. (1998, 2000) provide the only quantitative analyses we know of that depict this region of *post mortem* human brain continuously, rather than simply reporting integrated estimates over the entire amygdaloid complex. A qualitative comparison (Fig. 5) shows the most drastic difference in medial extent from our study, alongside expression patterns of the synthetic enzymes for glutamate and GABA. Over the approximate region of variation, a lateral to medial gradient is evident for glutamate and GABA synthetic capacity, likely indicating greater density of neural synapses and support cells (McKenna et al., 2000). Referencing the endorhinal sulcus and optic tract as readily visible landmarks that can be found on any MRI: the highest density appears around the apex of the sulcus, the region of the anterior amygdaloid area, and at the surface of the semilunar gyrus, the region of the cortical nucleus, which is bounded inferior-medially by the semiannular sulcus, a slight indentation identifiable by its proximity to the optic tract. Other microphotometry results by the same group show a very similar pattern of Choline acetyl-transferase expression and a single peak of overall cellularity (via Nissl stain) in the cortical nucleus region but not the anterior amygdaloid area (Sutoo et al., 1998). The two scans depicted (Figs. 5d,e) had the same LW (0.048 ppm), identical inferior extent, and very similar volume (2.152 mL vs 2.212 mL, respectively), but the spectrum acquired with more medial coverage estimated NAA to be 1.3 A.U. or 21% higher (13% after GM/WM correction by residualization), Cre was 2.2 A.U. or 43% higher (30% after GM/WM) and Cho was 0.54 or 24% higher (4% after GM/WM). SNR was 6 vs 8, respectively, due to increased NAA since the RMS residual (NAA/SNR) was .90 vs .89, respectively.

Since peak neuronal density is in the semilunar gyrus, average metabolite levels likely increase as the inferior extent of the MRS acquisition comes into register with the inferior limit of this neuron-dense region, potentially decreasing again as it surpasses and partially excludes this border. This qualitative observation could explain the non-linearity seen in our within-subject spatial analyses (Figs. 4d–f).

To explore this further, we attempted to use the semiannular sulcus, at the inferior-medial limit of this dense region, as a reference to test for anatomical gradients in neurochemistry in a between-subjects analysis (Figs. 5f–h). We found similar, albeit weaker, effects of medial and inferior extent as in our within-subjects analyses that once again were robust to covariates of SNR, LW and GM/WM (Table 6). A similar referencing to the superior-medial extent of the semilunar gyrus was far less robust (data not shown), as might be expected given that a variable amount of the gyrus extends beyond this point.

As before, we used a simple linear correction using group-estimated beta-weights to correct individual metabolite estimates, this time with reference to the semiannular sulcus, and recalculated reliability (Table 3). Accounting for differences in voxel medial and inferior border placement reduced the between-subject standard deviations by about 40% and reduced intraclass correlations to 0.56 for NAA and 0.52 for Cre (Table 3). Careful use of the landmarks of the optic tract, semiannular sulcus, and the extent of the endorhinal sulcus for precise localization may provide an amygdala-MRS protocol that is more sensitive to individual differences.

Ideal amygdala-MRS protocol

Based on the above findings, the ideal amygdala-MRS protocol would align the medial and inferior borders of the acquisition volume to the semiannular sulcus, thereby enveloping the synaptically dense semilunar gyrus and anterior amygdaloid area. Outer volume suppression pulses would saturate the corner closest to the auditory

Table 5
Within-individual variation in Medial and Inferior extent affect metabolite estimates even covarying spectral quality indices and tissue content.

Metabolite	Medial	Anterior	Inferior	SNR	LW[a]	GM/WM[b]
NAA	$\beta = 0.30$ $r_{semi} = 0.23$ $p = 0.11$	$\beta = -0.04$ $r_{semi} = -0.03$	$\beta = 0.44$ $r_{semi} = 0.34$ $p = 0.02$	$\beta = 0.24$ $r_{semi} = 0.21$ $p = 0.13$	$\beta = 0.01$ $r_{semi} = 0.01$	$\beta = 0.14$ $r_{semi} = 0.11$
Cre	$\beta = 0.61$ $r_{semi} = 0.46$ $p = 1 \times 10^{-4}$	$\beta = -0.10$ $r_{semi} = -0.08$	$\beta = 0.38$ $r_{semi} = 0.29$ $p = 0.01$	$\beta = 0.09$ $r_{semi} = 0.08$	$\beta = 0.02$ $r_{semi} = 0.02$	$\beta = 0.19$ $r_{semi} = 0.14$ $p = 0.20$
Cho	$\beta = 0.30$ $r_{semi} = 0.22$ $p = 0.04$	$\beta = -0.22$ $r_{semi} = -0.19$ $p = 0.07$	$\beta = 0.41$ $r_{semi} = 0.32$ $p = 0.004$	$\beta = 0.07$ $r_{semi} = 0.06$	$\beta = -0.16$ $r_{semi} = -0.13$	$\beta = -0.58$ $r_{semi} = 0.43$ $p = 2 \times 10^{-4}$
mI	$\beta = 0.26$ $r_{semi} = 0.19$	$\beta = 0.09$ $r_{semi} = 0.08$	$\beta = 0.35$ $r_{semi} = 0.27$ $p = 0.08$	$\beta = 0.17$ $r_{semi} = 0.15$	$\beta = 0.27$ $r_{semi} = 0.22$	$\beta = 0.03$ $r_{semi} = 0.02$
Glx	$\beta = 0.18$ $r_{semi} = 0.13$	$\beta = -0.30$ $r_{semi} = -0.25$ $p = 0.09$	$\beta = 0.47$ $r_{semi} = 0.36$ $p = 0.02$	$\beta = 0.49$ $r_{semi} = 0.43$ $p = 0.005$	$\beta = 0.26$ $r_{semi} = 0.21$ $p = 0.15$	$\beta = 0.00$ $r_{semi} = 0.00$

[a] Absolute difference in LW.
[b] Estimated gray matter/white matter ratio in acquisition volume; $p > 0.20$ not shown.

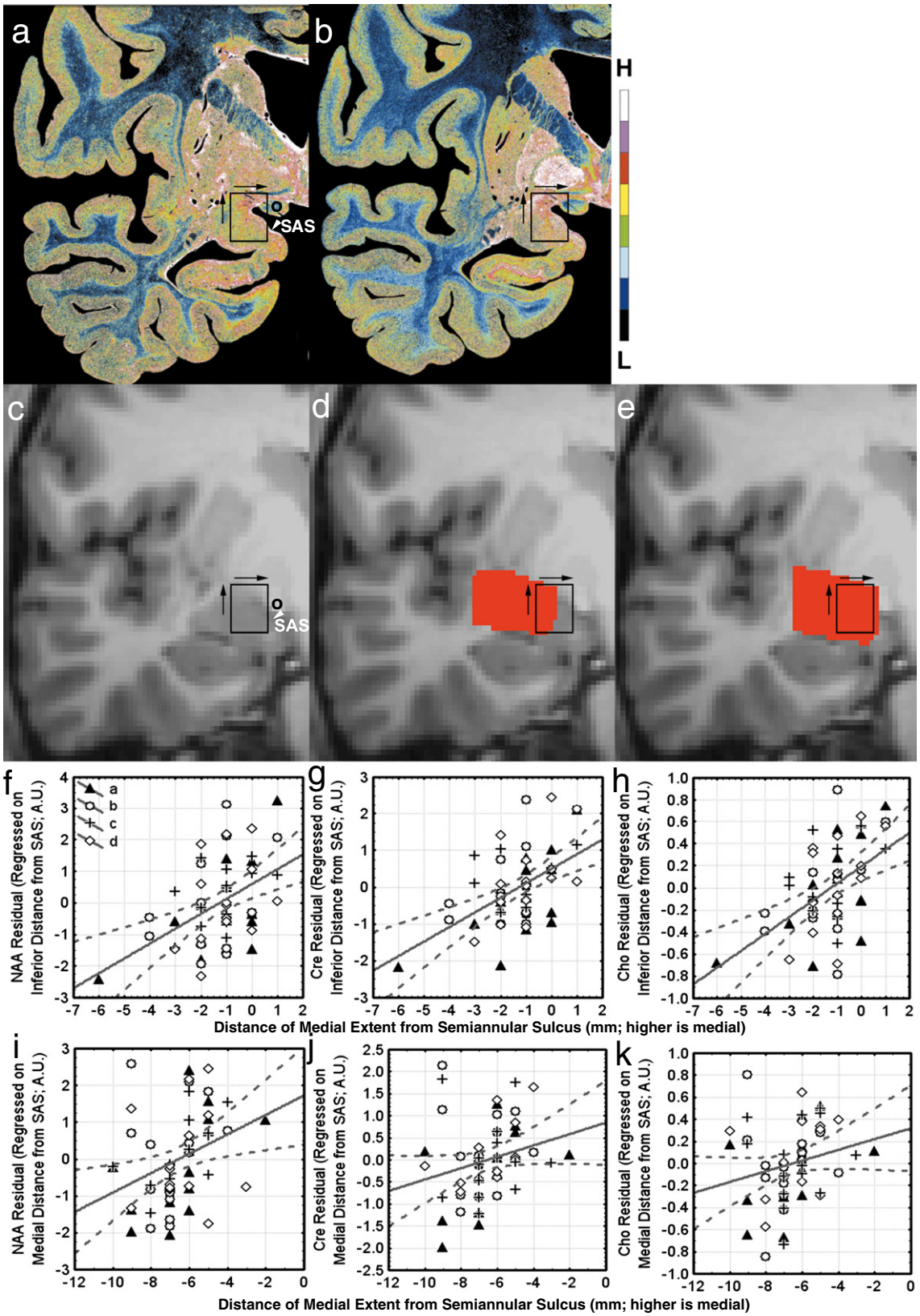

Fig. 5. Anatomical variation in amygdala-MRS metabolites parallels increased synaptic density around the endorhinal suclus of the human brain. Results of Sutoo et al. (2000) with approximate region of medial extent variability from our study (rectangle in a–e) overlying quantitative staining of glutamate dehydrogenase (GDH, a) and glutamic acid decarboxylase (GAD, b). More superiorly and medially, the density of GDH and GAD increases, indicating a likely increase in synaptic density. Example underlying anatomy (c) shows the easily-identified optic tract (*O*) near the semiannular sulcus (*SAS*, arrowhead) and largest within-individual shift in medial border of amygdala-MRS (4 mm; red) of all 56 sessions (d–e). Between-individual analysis reveals independent contributions of amygdala-MRS medial extent (f–h) and inferior extent (i–k) expressed as distance from the semiannular sulcus. Medial extent shows the predicted positive correlation with NAA (f, $r=0.46$, $p=4\times10^{-4}$; LW<0.06 ppm, 46 sessions: $r=0.39$, $p=0.008$), Cre (g, $r=0.52$, $p=4\times10^{-5}$; LW<0.06: $r=0.52$, $p=2\times10^{-4}$) and Cho (h, $r=0.50$, $p=1\times10^{-4}$; LW<0.06: $r=0.46$, $p=0.001$). Similarly for inferior extent with NAA (i, $r=0.34$, $p=0.01$; LW<0.06: $r=0.43$, $p=0.003$) and Cre (j, $r=0.24$, $p=0.07$; LW<0.06: $r=0.32$, $p=0.03$) with Cho at trend level (k, $r=0.22$, $p=0.10$; LW<0.06: $r=0.28$, $p=0.06$).

Table 6
Between-individual variation in medial and inferior extent relative to semiannular sulcus.

Metabolite	Medial	Inferior	SNR	LW	GM/WM[a]
NAA	$\beta = 0.37$ $r_{semi} = 0.31$ $p = 0.01$	$\beta = 0.40$ $r_{semi} = 0.34$ $p = 0.005$	$\beta = 0.22$ $r_{semi} = 0.18$ $p = 0.12$	$\beta = 0.25$ $r_{semi} = 0.23$ $p = 0.06$	$\beta = 0.12$ $r_{semi} = 0.10$
Cre	$\beta = 0.52$ $r_{semi} = 0.43$ $p = 3 \times 10^{-4}$	$\beta = 0.32$ $r_{semi} = 0.28$ $p = 0.01$	$\beta = 0.09$ $r_{semi} = 0.08$	$\beta = 0.35$ $r_{semi} = 0.32$ $p = 0.005$	$\beta = 0.12$ $r_{semi} = 0.10$
Cho	$\beta = 0.45$ $r_{semi} = 0.37$ $p = 0.001$	$\beta = 0.37$ $r_{semi} = 0.31$ $p = 0.004$	$\beta = 0.09$ $r_{semi} = 0.07$	$\beta = 0.43$ $r_{semi} = 0.39$ $p = 4 \times 10^{-4}$	$\beta = 0.30$ $r_{semi} = 0.25$ $p = 0.02$
mI	$\beta = 0.45$ $r_{semi} = 0.37$ $p = 0.004$	$\beta = 0.21$ $r_{semi} = 0.18$ $p = 0.15$	$\beta = 0.13$ $r_{semi} = 0.11$	$\beta = 0.07$ $r_{semi} = 0.06$	$\beta = 0.07$ $r_{semi} = 0.06$
Glx	$\beta = 0.18$ $r_{semi} = 0.15$	$\beta = 0.34$ $r_{semi} = 0.29$ $p = 0.01$	$\beta = 0.20$ $r_{semi} = 0.17$ $p = 0.14$	$\beta = 0.57$ $r_{semi} = 0.53$ $p = 3 \times 10^{-5}$	$\beta = 0.06$ $r_{semi} = 0.04$

[a] Estimated gray matter/white matter ratio in acquisition volume; $p > 0.20$ not shown.

canal and temporal bone airspaces, allowing a line width less than 0.06 ppm. Given the dependence of Cho on partial volume of gray matter/white matter, ideal measures would also include correction for GM/WM. To approximate this, we combined all three corrections for our best estimate of the true reliability of individual differences (ICC) for each metabolite (Table 3).

Our ideal reliability estimates NAA and Cre were in the moderate range, between 0.5 and 0.6. This technique is appropriate for measurements of amygdala neurochemistry in studies with high statistical power from larger sample sizes or multiple scan sessions, and for studies of diverse populations, such as developmental and disease state experiments, with larger expected between-subject differences. Further improvements in voxel definition and better spectral quality from longer scans or specialized pulse sequences may allow reliable measurement of more metabolites (especially Glx) and individual differences measurements in small, homogeneous populations.

Discussion

We present a well-defined technique to obtain spectra from the amygdala, exclusive of hippocampal head, foregoing standardized acquisition dimensions in favor of careful compensation for individual anatomy and field inhomogeneity to achieve such high spectral quality that individual spectra are on par with group-averaged data from other studies (Baker et al., 2008) and spectra acquired at 4T (Venkatraman et al., 2006). We identified an age-related contribution of internal auditory canal development to field inhomogeneity and quantitatively linked this to higher spectral quality in youth. By compensating for this, we reduced effects of age on spectral quality and gained more freedom to capture relevant anatomical boundaries. In a within-subject analysis across 4 sessions (56 scans), we find a striking sensitivity to anatomic variation, contributing in a metabolite-specific manner up to 29% of measurement variability. Correcting for this partial volume effect greatly improves within-subject consistency, making combination of data across sessions much more feasible. Partial voluming of cortical and anterior amygdaloid areas also contaminates between-subject variability, suggesting that an amygdala-MRS prescription with medial and inferior extent aligned to the semiannular sulcus could prove more sensitive to true individual differences in amygdala neurochemistry. We find that the combination of LW < 0.06 ppm, spatial correction to the semiannular sulcus and correction for GM/WM produces moderately reliable individual differences measurements of NAA and Cre in healthy adult populations.

To our knowledge, this is the first study to obtain reliable measurement of amygdala-specific neurochemistry in vivo. In comparison with other reliability studies in medial temporal lobe, we achieved better line widths and within-subject coefficients of variation than a much larger volume (8 mm^3) over the middle third of hippocampus (Wellard et al., 2005). Schubert et al. (2004) estimated reliability of a 12 mm^3 volume over middle and posterior hippocampus in a larger sample ($n = 39$) over 4 weeks; they report the less-stringent pearson correlation, which was quite good for Cho (0.79) but only modest for NAA (0.42) and insignificant for Cre (unreported). The only study to attempt an amygdala-specific protocol (Hoerst et al., 2009) centered a very small and invariant acquisition volume (1.4 cm^3) within the amygdala, leading to insufficient spectral quality to resolve key resonances. Numerous studies have attempted amygdala MRS in autistic samples (Endo et al., 2007; Gabis et al., 2008; Kleinhans et al., 2009; Otsuka et al., 1999; Page et al., 2006) with intriguing findings, but spectral quality was inferior or inadequately reported, hippocampal head was partially and variably included, and reliability of these techniques was not established.

Like Wellard et al. (2005), we found mI and Glx to have the highest within-subject variability. These less abundant metabolites are difficult to measure due to coupling and peak overlap, so we aimed for the best possible reliability of the major metabolites with the eventual goal of using specialized spectral editing techniques and more acquisitions to examine neurotransmitter levels.

We found age-related changes in internal auditory canal to underlie the surprising ease of amygdala-MRS acquisition in children. Our finding that the internal auditory canal produced severe and potentially unshimmable distortions in the middle third of hippocampus suggests that minor metabolites may not be reliably measurable in this region. Furthermore, the age-related change in skull airspaces may affect other types of magnetic resonance imaging including fMRI and EPI-based DTI sequences.

A potential limitation of our technique is that the small, anatomically-localized acquisition is more vulnerable to effects of motion, although its central location reduces the net displacement. To achieve the SNR required for analysis of minor metabolites, multiple acquisitions with interleaved anatomical localizers or novel prospective motion correction algorithms may be required. Our findings of an anatomical landmark that can greatly reduce between-session variability for a given individual should also facilitate combining across multiple acquisitions on different days to achieve the necessary SNR.

Another limitation is that our spectra were not fully relaxed, nor did we attempt to calculate absolute concentrations of metabolites and there remains a possibility that individuals stably differ in relaxation time, thereby enhancing our ICCs. Future studies with multiple echo times could resolve this.

We also found a novel sensitivity to spatial positioning that seems to parallel differences in synaptic density and cellularity. Our data suggest that specifying the details of voxel placement is at least as important as correcting for tissue (GM/WM) composition for achieving reliable MRS measurements of amygdala neurochemistry. Further

prospective study of MRS sensitivity to synaptic density with histological correlation would be useful.

Despite these limitations, we developed an amygdala-specific MRS technique that produces comparable spectra in children and adults and is sensitive to stable differences in neurochemistry between healthy individuals. The robustness across adolescent development could facilitate identification of neurochemical signatures or biomarkers of neural maturation in this late-developing emotional center.

Supplementary materials related to this article can be found online at doi:10.1016/j.neuroimage.2011.08.090.

Acknowledgment

We would like to thank all of the individuals and families that participated in our studies. Funding for this project provided by a P30 award (HD03352) to the Waisman Center for Developmental Disabilities (Dr. Davidson, imaging core project PI), a Conte Neuroscience Center from the National Institute of Mental Health (P50-MH084051PI: RJ Davidson), as well as an R03 award to Dr. Dalton (MH082267) and a Ruth Kirschstein NRSA to Dr. Nacewicz (MH081467) from the National Institute of Mental Health. The funding sources had no involvement in study design, in collection, analysis, interpretation or write up of data, or in the decision to submit the work for publication.

References

Adolphs, R., Gosselin, F., Buchanan, T.W., Tranel, D., Schyns, P., Damasio, A.R., 2005. A mechanism for impaired fear recognition after amygdala damage. Nature 433, 68–72.
Ambroggi, F., Ishikawa, A., Fields, H.L., Nicola, S.M., 2008. Basolateral amygdala neurons facilitate reward-seeking behavior by exciting nucleus accumbens neurons. Neuron 59, 648–661.
Baker, E.H., Basso, G., Barker, P.B., Smith, M.A., Bonekamp, D., Horska, A., 2008. Regional apparent metabolite concentrations in young adult brain measured by (1)H MR spectroscopy at 3 Tesla. J. Magn. Reson. Imaging 27, 489–499.
Brierley, B., Shaw, P., David, A.S., 2002. The human amygdala: a systematic review and meta-analysis of volumetric magnetic resonance imaging. Brain Res. Brain Res. Rev. 39, 84–105.
Cox, R.W., 1996. AFNI: software for analysis and visualization of functional magnetic resonance neuroimages. Comput. Biomed. Res. 29, 162–173.
Dalton, K.M., Nacewicz, B.M., Johnstone, T., Schaefer, H., Gernsbacher, M.A., Goldsmith, H.H., Alex, E.A., Davidson, R.J., 2005. Gaze fixation and the neural circuitry of face processing in autism. Nat. Neurosci. 8, 519–526.
Davis, M., Whalen, P.J., 2001. The amygdala: vigilance and emotion. Mol. Psychiatry 6, 13–34.
Drost, D.J., Riddle, W.R., Clarke, G.D., 2002. Proton magnetic resonance spectroscopy in the brain: report of AAPM MR Task Group #9. Med. Phys. 29, 2177–2197.
Endo, T., Shioiri, T., Kitamura, H., Kimura, T., Endo, S., Masuzawa, N., Someya, T., 2007. Altered chemical metabolites in the amygdala-hippocampus region contribute to autistic symptoms of autism spectrum disorders. Biol. Psychiatry 62, 1030–1037.
Frodl, T., Meisenzahl, E.M., Zetzsche, T., Born, C., Jäger, M., Groll, C., Leinsinger, R.B.G., Möller, H.-J., 2003. Larger amygdala volumes in first depressive episode as compared to recurrent major depression and healthy control subjects. Biol. Psychiatry 53, 338–344.
Gabis, L., Wei, H., Azizian, A., DeVincent, C., Tudorica, A., Kesner-Baruch, Y., Roche, P., Pomeroy, J., 2008. 1H-magnetic resonance spectroscopy markers of cognitive and language ability in clinical subtypes of autism spectrum disorders. J. Child Neurol. 23, 766–774.
Geurts, J.J., Barkhof, F., Castelijns, J.A., Uitdehaag, B.M., Polman, C.H., Pouwels, P.J., 2004. Quantitative 1H-MRS of healthy human cortex, hippocampus, and thalamus: metabolite concentrations, quantification precision, and reproducibility. J. Magn. Reson. Imaging 20, 366–371.
Giedd, J.N., Castellanos, F.X., Rajapakse, J.C., Vaituzis, A.C., Rapoport, J.L., 1997. Sexual dimorphism of the developing human brain. Prog. Neuropsychopharmacol. Biol. Psychiatry 21, 1185–1201.
Giedd, J.N., Vaituzis, A.C., Hamburger, S.D., Rajapakse, N.L.J.C., Kaysen, D., Vauss, Y.C., Rapoport, J.L., 1996. Quantitative MRI of the temporal lobe, amygdala, and hippocampus in normal human development: ages 4–18 years. J. Comp. Neurol. 366, 223–230.
Hoerst, M., Weber-Fahr, W., Tunc-Skarka, N., Ruf, M., Bohus, M., Schmahl, C., Ende, G., 2009. Metabolic alterations in the amygdala in borderline personality disorder: a proton magnetic resonance spectroscopy study. Biol. Psychiatry 67, 399–405.
Kleinhans, N.M., Johnson, L.C., Richards, T., Mahurin, R., Greenson, J., Dawson, G., Aylward, E., 2009. Reduced neural habituation in the amygdala and social impairments in autism spectrum disorders. Am. J. Psychiatry 166, 467–475.
Kreis, R., 2004. Issues of spectral quality in clinical 1H-magnetic resonance spectroscopy and a gallery of artifacts. NMR Biomed. 17, 361–381.
McEwen, B.S., 2003. Mood disorders and allostatic load. Biol. Psychiatry 54, 200–207.
McEwen, B.S., 2007. Physiology and neurobiology of stress and adaptation: central role of the brain. Physiol. Rev. 87, 873–904.
McKenna, M.C., Stevenson, J.H., Huang, X., Hopkins, I.B., 2000. Differential distribution of the enzymes glutamate dehydrogenase and aspartate aminotransferase in cortical synaptic mitochondria contributes to metabolic compartmentation in cortical synaptic terminals. Neurochem. Int. 37, 229–241.
Mitra, R., Jadhav, S., McEwen, B.S., Vyas, A., Chattarji, S., 2005. Stress duration modulates the spatiotemporal patterns of spine formation in the basolateral amygdala. Proc. Natl. Acad. Sci. U.S.A. 102, 9371–9376.
Mueller-Lisse, U.G., Scherr, M.K., 2007. Proton MR spectroscopy of the prostate. Eur. J. Radiol. 63, 351–360.
Munson, J., Dawson, G., Abbott, R., Faja, S., Webb, S.J., Friedman, S.D., Shaw, D., Artru, A., Dager, S.R., 2006. Amygdalar volume and behavioral development in autism. Arch. Gen. Psychiatry 63, 686–693.
Nacewicz, B.M., Dalton, K.M., Johnstone, T., Long, M.T., McAuliff, E.M., Oakes, T.R., Alexander, A.L., Davidson, R.J., 2006. Amygdala volume and nonverbal social impairment in adolescent and adult males with autism. Arch. Gen. Psychiatry 63, 1417–1428.
Oler, J.A., Fox, A.S., Shelton, S.E., Rogers, J., Dyer, T.D., Davidson, R.J., Shelledy, W., Oakes, T.R., Blangero, J., Kalin, N.H., 2010. Amygdalar and hippocampal substrates of anxious temperament differ in their heritability. Nature 466, 864–868.
Otsuka, H., Harada, M., Mori, K., Hisaoka, S., Nishitani, H., 1999. Brain metabolites in the hippocampus-amygdala region and cerebellum in autism: an 1H-MR spectroscopy study. Neuroradiology 41, 517–519.
Oz, G., Terpstra, M., Tkac, I., Aia, P., Lowary, J., Tuite, P.J., Gruetter, R., 2006. Proton MRS of the unilateral substantia nigra in the human brain at 4 tesla: detection of high GABA concentrations. Magn. Reson. Med. 55, 296–301.
Page, L.A., Daly, E., Schmitz, N., Simmons, A., Toal, F., Deeley, Q., Ambery, F., McAlonan, G.M., Murphy, K.C., Murphy, D.G., 2006. In vivo 1H-magnetic resonance spectroscopy study of amygdala-hippocampal and parietal regions in autism. Am. J. Psychiatry 163, 2189–2192.
Port, J.D., Unal, S.S., Mrazek, D.A., Marcus, S.M., 2008. Metabolic alterations in medication-free patients with bipolar disorder: a 3T CSF-corrected magnetic resonance spectroscopic imaging study. Psychiatry Res. 162, 113–121.
Provencher, S.W., 1993. Estimation of metabolite concentrations from localized in vivo proton NMR spectra. Magn Reson Med 30, 672–679.
Rojas, D.C., Smith, J.A., Benkers, T.L., Camou, S., Reite, M.L., Rogers, S.J., 2004. Hippocampus and amygdala volumes in parents of children with autistic disorder. Am. J. Psychiatry 161, 2038–2044.
Schubert, F., Gallinat, J., Seifert, F., Rinneberg, H., 2004. Glutamate concentrations in human brain using single voxel proton magnetic resonance spectroscopy at 3 Tesla. Neuroimage 21, 1762–1771.
Schumann, C.M., Hamstra, J., Lotspeich, B.L.G.-J.L.J., Kwon, H., Lammers, M.H.B.A.R., Reiss, A.L., Amaral, D.G., 2004. The amygdala is enlarged in children but not adolescents with autism; the hippocampus is enlarged at all ages. J. Neurosci. 24, 6392–6401.
Shrout, P.E., Fleiss, J.L., 1979. Intraclass correlations: uses in assessing rater reliability. Psychol. Bull. 86, 420–428.
Sutoo, D., Akiyama, K., Yabe, K., 1998. Quantitative mapping analyzer for determining the distribution of neurochemicals in the human brain. J. Neurosci. Methods 85, 161–173.
Sutoo, D., Akiyama, K., Yabe, K., 2000. Quantitative maps of GAbAergic and glutamatergic neuronal systems in the human brain. Hum. Brain Mapp. 11, 93–103.
Tomarken, A.J., Davidson, R.J., Wheeler, R.E., Doss, R.C., 1992. Individual differences in anterior brain asymmetry and fundamental dimensions of emotion. J. Pers. Soc. Psychol. 62, 676–687.
van Eijndhoven, P., van Wingen, G., van Oijen, K., Rijpkema, M., Goraj, B., Jan Verkes, R., Oude Voshaar, R., Fernandez, G., Buitelaar, J., Tendolkar, I., 2009. Amygdala volume marks the acute state in the early course of depression. Biol. Psychiatry 65, 812–818.
Velakoulis, D., Wood, S.J., Wong, M.T., McGorry, P.D., Yung, A., Phillips, L., Smith, D., Brewer, W., Proffitt, T., Desmond, P., Pantelis, C., 2006. Hippocampal and amygdala volumes according to psychosis stage and diagnosis: a magnetic resonance imaging study of chronic schizophrenia, first-episode psychosis, and ultra-high-risk individuals. Arch. Gen. Psychiatry 63, 139–149.
Venkatraman, T.N., Hamer, R.M., Perkins, D.O., Song, A.W., Lieberman, J.A., Steen, R.G., 2006. Single-voxel 1H PRESS at 4.0T: precision and variability of measurements in anterior cingulate and hippocampus. NMR Biomed. 19, 484–491.
Wellard, R.M., Briellmann, R.S., Jennings, C., Jackson, G.D., 2005. Physiologic variability of single-voxel proton MR spectroscopic measurements at 3T. AJNR Am. J. Neuroradiol. 26, 585–590.